INTERNATIONAL JOURNAL OF HYDROGEN ENERGY 48 (2023) 7499–7514

Available online at www.sciencedirect.com

ScienceDirect

journal homepage: www.elsevier.com/locate/he

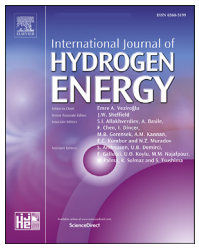

Critical verification of the effective diffusion concept

Andreas Drexler [a,*], *Matthew Galler* [b], *Hamdi Elsayed* [a], *Rudolf Vallant* [a], *Christof Sommitsch* [a]

[a] *Graz University of Technology, Institute of Materials Science, Joining and Forming, Research Group of Lightweight and Forming Technologies, Inffeldgasse 11/I, 8010 Graz, Austria*

[b] *Voestalpine Wire Rod Austria, Drahtstraße 1, 8792 St. Peter-Freienstein, Austria*

HIGHLIGHTS

- FDM is presented to simulate permeation and diffusion depth profiles.
- The effective diffusion coefficient strongly depends on the charging conditions.
- The characteristic diffusion depth correlates with $\sqrt{t}$, but not with $\sqrt{D_{eff}}$.
- The basic assumption of the effective diffusion concept is violated.

ARTICLE INFO

Article history:
Received 25 June 2022
Received in revised form
7 November 2022
Accepted 9 November 2022
Available online 8 December 2022

Keywords:
Hydrogen
Diffusion
Trapping
Diffusion depth
Numerical modelling
Simulation

ABSTRACT

Knowing the hydrogen distribution $c(x,t)$ and local hydrogen concentration gradients $\mathrm{grad}(c)$ in ferritic steel components is crucial with respect to hydrogen embrittlement. Basically, hydrogen is absorbed from corrosive or gaseous environments via the surface and diffuses through interstitial lattice sites into bulk. Although, the lattice diffusion coefficient $D_L \sim 0.01\,mm^2/s$ is in the order of magnitude of those for well-annealed pure iron, trapping sites in the microstructure retard the long-range chemical diffusion $j_L = -D_{chem}(c)\mathrm{grad}(c)$, causing local hydrogen accumulation in near surface regions in limited time. Considering pure ferritic crystals without trapping sites in the microstructure, the limited characteristic diffusion depth $x_c \sim \sqrt{D_{eff}t}$ is proportional to the square root of the effective diffusion coefficient D_{eff} and of time t. Effective diffusion coefficients are measured independently for hydrogen using the electrochemical permeation technique. For pure crystals, the effective diffusion coefficient is constant at given temperature and allows accurate calculations of the diffusion depths. However, with trapping sites in the microstructure the effective diffusion coefficient is not a material property anymore and becomes dependent on the hydrogen charging conditions. In the present work, the theory of hydrogen bulk diffusion is used to verify the concept of effective diffusion. For that purpose, the generalized bulk diffusion equation was solved numerically by using the finite difference method (FDM). The implementation was checked using analytical solutions and a comprehensive convergence study was done to avoid mesh and time dependency of the results. It is shown that effective diffusion coefficients can vary by magnitudes depending

* *Corresponding author.*
E-mail address: andreas.drexler@tugraz.at (A. Drexler).

https://doi.org/10.1016/j.ijhydene.2022.11.105

on the sub-surface lattice concentration. This limits the application of the effective diffusion concept and also the calculation of the characteristic diffusion depth.

Introduction

Understanding hydrogen diffusion in metals is crucial to develop improved mitigation strategies for hydrogen embrittlement (HE) [1]. For example, micrometre thick coatings [2] can repel hydrogen atoms by making hydrogen absorption strongly endothermic and lower permeation rates to bulk [3–5]. Another example is beneficial trapping sites in the microstructure, like titanium or vanadium carbides [6], which are known to reduce bulk diffusivity [6–8] causing limited hydrogen diffusion depths and thus hydrogen concentration gradients grad(c) in final components [9]. Polyanskiy et al. [10,11] studied the role of local hydrogen accumulation in surface-near regions and named this phenomenon "skin-effect".

It is believed that hydrogen diffusion from the bulk to crack tips [12–14] is one of the main driving forces of hydrogen assisted crack (HAC) growth. Critical hydrogen sources are available in corrosive or gaseous environments [15] all along the production lines of steel components and during service. Once absorption occurred, atomic hydrogen [16] diffuses inside the components until a stationary distribution is reached. The absorbed hydrogen content can be measured by thermal desorption analysis (TDA) methods. However, TDA only allows measurement of the total hydrogen content as a function of the sample weight. Inhomogeneous hydrogen distributions, which result from inhomogeneous strain distributions in the components [17,18] or limited diffusion time, are not represented by using the TDA method.

Other interstitial elements in ferritic steels, such as carbon or nitrogen, allow a more direct experimental observation of the element distribution. Case hardening of gears is a well-known example, where the diffusion depth profile of carbon in steels can be measured directly in the cross-section of the component using indentation techniques. It is well known that diffusion depth of carbon atoms scales with the square root of time $\sqrt{t}$. Different to carbon, the increase of hardness by hydrogen [19] in ferritic steels is not large enough to prove the time dependency directly in the cross-section of a component. Furthermore, the fugacity of hydrogen is very high and makes indentation measurements under atmospheric conditions very difficult. Therefore, numerical or analytical methods are necessary to predict local hydrogen distributions and diffusion depths from independent measurements, such as electrochemical permeation or TDA [20,21].

For determining the characteristic diffusion depth x_c, the generalized diffusion equation [22,23] must be solved either analytically or numerically. An analytical solution exists for semi-infinite volumes in case of pure metals without trapping sites. In this case the characteristic diffusion depth $x_c \sim \sqrt{D_{eff} t}$ is much less than the thickness of the plate and increases linearly with the square root of the effective diffusion coefficient D_{eff} and the diffusion time t. The method of choice to measure hydrogen diffusion coefficients in steels is electrochemical permeation [20,24–27]. Devanathan and Stachurski [28] suggested to place a thin sample between two electrochemical cells, namely reduction and oxidation cell. On the reduction side, the sample surface is cathodically polarized to produce adsorbed hydrogen atoms according to the Volmer reaction. After absorption, hydrogen permeates bulk and is oxidized on the other side of the sample. The permeation time, which is a measure for hydrogen bulk diffusivity, depends not only on the investigated microstructure, but also on the hydrogen charging conditions and the sample thickness. According to Wipf [16], the hydrogen permeation rate is generally more influenced by trapping than by the value of the diffusion coefficient D_L of interstitial lattice hydrogen. Drexler et al. [2] proved experimentally and numerically for dual phase (DP) steels that the permeation time strongly depends on the sub-surface lattice concentration at the reduction side. In other words, the permeation time decreases with increasing stationary current density, as it was experimentally shown by Darken and Smith [29] in 1949 or later by Zafra et al. [26]. However, this dependencies of the effective diffusion coefficients are not considered in nowadays standards, such as ASTM [30] or EN ISO [31], and hence, measured effective diffusion coefficients D_{eff} have been used extensively in literature

- for calculating the hydrogen diffusion distances in the microstructure during hydrogen assisted crack (HAC) growth [32–34],
- for correlating HE susceptibility indices with the diffusion distance [35,36],
- for estimating the minimum hydrogen charging time $t \sim L^2/2D_{eff}$ to reach hydrogen saturation before testing the HE susceptibility [37], with $L/2$ being the halve sample thickness or
- to study the effect of trapping sites on the bulk hydrogen diffusion [25,38,39].

Recently, M. Rhode et al. [40] applied the same equation to calculate the minimum waiting time t of as-welded plates to desorb hydrogen and to avoid hydrogen induced cracking (HIC).

The present work is dedicated to the critical verification of the effective diffusion concept and the characteristic diffusion depth in the presence of trapping sites in the microstructure. For that purpose, the theory of effective diffusion was compared with the more advanced theory of bulk hydrogen diffusion [23]. The generalized bulk diffusion equation [41] was solved numerically using the finite difference method (FDM). The numerical implementation was checked by

comparing with analytical solutions and a comprehensive convergence study was applied to guarantee simulation results independent of the chosen node density and time increment. Effective diffusion coefficients were simulated as function of the sub-surface lattice concentration and thickness and were compared with measured values from literature. Finally, hydrogen diffusion profiles in semi-infinite volumes were simulated and the characteristic diffusion depth was evaluated with respect to the effective diffusion coefficients and time.

Theory

The following section summarizes the theoretical background of hydrogen bulk diffusion and effective diffusion in ferritic crystal structures. Analytical solutions are provided for diffusion in semi-infinite volumes and plane sheets.

Basic equation for bulk diffusion

Hydrogen atoms occupy either interstitial lattice sites or trap at microstructural defect sites in ferritic crystal structures. Therefore, the total hydrogen concentration c can be separated as

$$c = c_L + c_T, \tag{1}$$

where c_L is the lattice concentration and c_T is the trapped hydrogen concentration, respectively. At room temperature the lattice site fraction y_L, which is the ratio of lattice concentration c_L and lattice site density N_L, is

$$y_L = c_L/N_L << 1 \tag{2}$$

and most of the total hydrogen concentration is trapped at microstructural defect sites [42]. Hydrogen trapping sites are classified according to their binding energy E_b [43] and trap density N_T. The binding energy arises from both the elastic expansion of the crystal lattice around microstructural defects [12,13] and the atomic bond between hydrogen and the iron atoms of the host metal [44,45]. Typical binding energies in ferritic iron range up to around 100 kJ/mol with binding energies below 50 kJ/mol being named “shallow” trapping sites and above 50 kJ/mol being named “deep” trapping sites [46]. In thermodynamic equilibrium binding energies of 60 kJ/mol or higher cause a full occupation of the trapping sites at room temperature [44] and an increase of the binding energy would not change the trap site fraction $y_T \cong 1$. The difference in binding energy becomes visible during linear heating, as it is used in the thermal desorption spectroscopy (TDS) measurements [47]. Typical trap densities N_T range from 10^{-12} to 10^{-6} mol/mm^3 [7,8,24] and seem to be lower the higher the binding energy E_b. Nevertheless, a detailed characterization of the available trapping sites with respect to their binding energy and trap density makes model-based evaluation of TDS spectra [2,7,8,48] or permeation curves [24,49] necessary.

A long lasting discussion in literature on the calculation of trapped hydrogen concentrations ranges back to McNabb and Foster [50] or Oriani [51] in the early 60ies and 70ies. Since then, several more generalized bulk diffusion models have been derived [7,22,41,46]. While McNabb and Foster assumed the trapping kinetics as one of the main retardation mechanisms during bulk diffusion, the local equilibrium theory, which was first suggested by Oriani [41] and later generalized by Svoboda and Fischer [41], assumes local equilibrium between lattice and trapped hydrogen atoms as following

$$c_T = \frac{y_L N_T}{K + y_L(1-K)} \tag{3}$$

where $K = \exp(-E_b/R_g T)$ is the equilibrium constant, R_g is the universal gas constant and T is the temperature. Care must be taken on the distribution of trapping sites in the microstructure whenever kinetic theories instead of equilibrium theories are applied. Raina et al. [48,49] were one of the first showing that Oriani's trapping approach gives reasonable agreement between simulation and measurements for permeation as well as TDS. Drexler et al. [2,7] validate Oriani's theory twice by comparing measurements and simulations and showed recently [2] that it is possible to describe measured TDS spectra as well as permeation transients of the same class of material with one constant set of trapping parameters. According to Toribio and Kharin [22] local equilibrium is reached, whenever long range chemical diffusion last much longer than reaching local equilibrium by microstructural relaxation between lattice and trapped hydrogen. For example, comparing the permeation times of well-annealed iron samples of around 10 s [25] with the permeation times of typical advanced high-strength steels of several hours [26,27], supports Oriani's theory of trapped hydrogen concentration. Furthermore, Kissinger's theory for the evaluation of single or well-separated TDS peaks [52] can be derived from Oriani's trapping theory [23,52]. Kirchheim [23] showed that the activation energy according to Kissinger's theory is more likely the activation energy of hydrogen bulk diffusion [52] rather than the desorption energy of individual trapping sites.

According to Fick's first law of diffusion, the lattice flux j_L is proportional to the gradient in lattice hydrogen concentration as

$$j_L = -D_L \mathrm{grad}(c_L) \tag{4}$$

where grad is the gradient operator in the actual configuration. $D_L = D_0 \exp(E_m/R_g T)$ is the lattice diffusion coefficient and D_0 is the jump frequency. E_m is the migration energy of lattice hydrogen, which is around 5 kJ/mol for ferritic iron [53–55]. Other driving forces were not considered in the present work, like mechanical, thermal, electrical or trap mobility [16,56]. Regarding hydrogen diffusion along interconnected trapping sites, Siegl et al. [25] could not measure any increase of the effective diffusion coefficient D_{eff} by altering grain size d_G and dislocation density ρ_D in pure iron, performing permeation measurements. In addition, the migration energies for hydrogen diffusion along grain boundaries were calculated to range from 8 to 31 kJ/mol [57]. Both the rather high migration energy $E_{m,T}$ with respect to the migration energy of lattice diffusion and the experimental observation let the authors assume that the trap flux along grain boundaries and dislocation can be neglected [24,25].

The mass balance for hydrogen must be reformulated concerning lattice sites, trapping sites and the lattice flux j_s [22,41] as

$$\frac{dc}{dt}=\frac{dc_L}{dt}+\frac{dc_T}{dt}=-\operatorname{div}(j_L) \tag{5}$$

where div is the divergence operator in the actual configuration and t is time. By considering Eq. (3) for trapped hydrogen concentration, Eq. (5) can be regarded as the generalized bulk diffusion equation for hydrogen. The rather complicated structure of Eq. (5) prompted the introduction of the chemical diffusion coefficient concept [41], which relates the diffusion flux with the gradient of the total hydrogen concentration c instead of the lattice hydrogen concentration c_L as following

$$j_L=-D_L\frac{dc_L}{dc}grad(c)=-D_{chem}(c)\mathrm{grad}(c) \tag{6}$$

The chemical diffusion coefficient D_{chem} differs form the lattice diffusion coefficient D_L in Eq. (4) being concentration dependent. According to Svoboda and Fischer [41,58] an analytical equation exists for single trapping sites:

$$D_{chem}=\frac{D_L}{2}\left(1+\frac{\frac{c}{N_L}(1-K)-\frac{N_T}{N_L}+K}{\sqrt{\left(\frac{c}{N_L}(1-K)-K-\frac{N_T}{N_L}\right)^2+\frac{4cK}{N_L}(1-K)}}\right) \tag{7}$$

Inserting this relation, yields the generalized bulk diffusion equation expressed in the actual local value of c:

$$\frac{dc}{dt}=\operatorname{div}(D_{chem}grad(c)) \tag{8}$$

Basic equation for effective diffusion

The effective diffusion concept, which is widely used in the field of electrochemical hydrogen permeation, bases on the generalized bulk diffusion equation given in Eq. (5) as following

$$\frac{dc_L}{dt}+\frac{dc_T}{dt}=\left(1+\frac{\partial c_L}{\partial c_T}\right)\frac{dc_L}{dt}=div(D_Lgrad(c_L)) \tag{9}$$

Based on the assumption that $\frac{\partial c_L}{\partial c_T}$ is space independent, Eq. (9) can be reformulated as

$$\frac{dc_L}{dt}=\frac{1}{1+\frac{\partial c_L}{\partial c_T}}div(D_Lgrad(c_L))=div\left(\frac{D_L}{1+\frac{\partial c_L}{\partial c_T}}grad(c_L)\right) \tag{10}$$

With $j_L=-D_{eff}grad(c_L)$ the space independent effective diffusion coefficient can be set as

$$D_{eff}=\frac{D_L}{1+\frac{\partial c_L}{\partial c_T}}=\frac{L^2}{n_D t_{lag}} \tag{11}$$

Different procedure exists in literature [59,60] to determine the effective diffusion coefficient from recorded permeation transients $j_L(t)$, with L being the sample thickness and n_D being a constant factor. They are all based on the effective diffusion concept and differ in the definition of the timelag and thus of the constant factor. According to the EN ISO standard [31] for electrochemical permeation measurements, the timelag t_{lag} is defined as the time necessary to reach 63% of the stationary flux $j_{L,S}$ and $n=6$.

Analytical solutions

Analytical solutions of the diffusion equation exist for semi-infinite volumes and plane sheets made out of pure crystals [61], which do not contain hydrogen trapping sites N_T. Dirichlet boundary conditions are considered as follows

$$c_L(x=0,t\geq 0)=c_{L,0} \tag{12}$$

and the initial hydrogen concentration $c_L(x>0,t=0,)=0$ is assumed to be zero in bulk.

Diffusion in a semi-infinite volume

The solution of classical Fick's law of diffusion yields the lattice hydrogen concentration as a function of space x and time t as

$$c_L(x,t)=c_{L,0}\left(1-\frac{2}{\sqrt{\pi}}\int_0^{\frac{x}{2\sqrt{D_Lt}}}e^{-x'^2}dx'\right). \tag{13}$$

Using the complementary error function known as $\mathrm{erfc}(z)=1-\frac{2}{\sqrt{\pi}}\int_0^z e^{-y^2}dy$, Eq. (13) can be reformulated to the well-known solution of the lattice hydrogen concentration profile as

$$c_L(x,t)=c_{L,0}\mathrm{erfc}\left(\frac{x}{2\sqrt{D_Lt}}\right). \tag{14}$$

For defining the characteristic diffusion depth x_c, Eq. (14) is derived with respect to space, yielding

$$\frac{dc_L}{dx}(x=0,t)=-\frac{2}{\sqrt{\pi}}c_{L,0}e^{-\frac{x^2}{4D_Lt}}\frac{1}{2\sqrt{D_Lt}}\Big|_{x=0}=-\frac{c_{L,0}}{\sqrt{\pi D_Lt}} \tag{15}$$

With the introduction of the tangent equation as

$$y(x,t)=\frac{c_{L,0}}{\sqrt{\pi D_Lt}}x+c_{L,0} \tag{16}$$

the characteristic diffusion depth x_{c_L} for pure crystals at $y=0$ follows as

$$x_{c_L}=\sqrt{\pi D_Lt} \tag{17}$$

A graphical interpretation of Eq. (16) and x_{c_L} is presented as dotted red line in Fig. 2b. According to Eq. (17), x_{c_L} in pure crystals at a given temperature is

- independent on the boundary condition $c_{L,0}$,
- increases by the square root of the diffusion time $\sqrt{t}$ and
- depends on the constant lattice diffusion coefficient D_L.

Diffusion in a plane sheet

In the case of hydrogen permeation through a thin sheet with a thickness of L, the lattice concentration changes according to

$$c_L(x,t)=c_{L,0}\left(1-\frac{x}{L}\right)+\frac{2}{\pi}\sum_{n=1}^{\infty}-\frac{c_{L,0}}{n}\sin\left(\frac{n\pi x}{L}\right)\exp\left(-\frac{D_Ln^2\pi^2t}{L^2}\right) \tag{18}$$

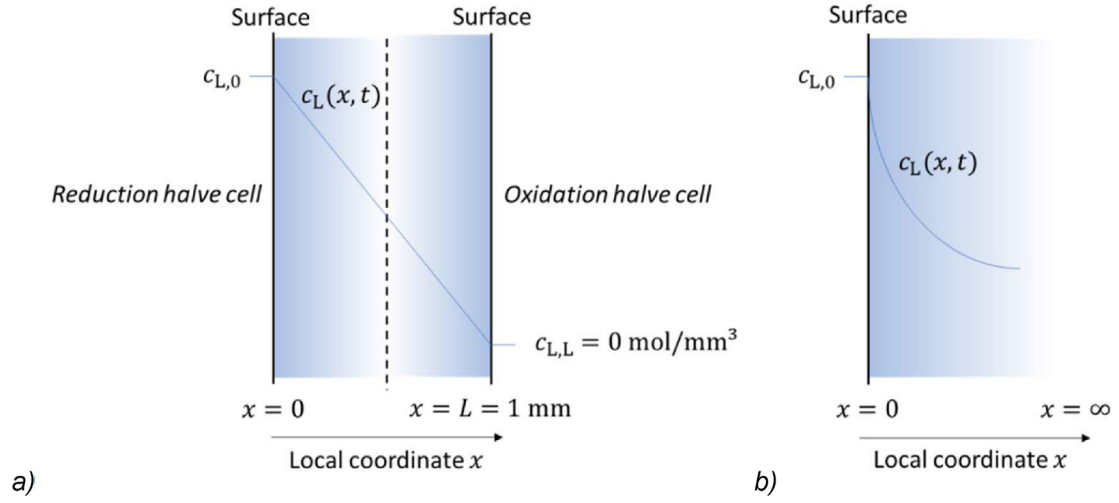

Fig. 1 – Sketch of the one-dimensional diffusion models: a) plane sheet model and b) semi-infinite volume model.

With increasing time, the solution of Eq. (18) approaches the stationary solution with a linear lattice concentration distribution, as illustrated in Fig. 1.

Hydrogen bulk diffusion modelling

In the following, all details are presented, which are required for setting up a finite difference model (FDM) implementation of the proposed bulk diffusion equation, which is given in Eq. (5). The models are formulated on the macroscale based on thermodynamic expressions [22,23,41] reassembling the mechanisms on the microscale.

Numerical solutions

The generalized bulk diffusion equation in one dimensional form is given in Cartesian coordinates as

$$\left(1+\frac{\partial c_T}{\partial c_L}\right)\frac{dc_L}{dt} = D_L\frac{\partial^2 c_L}{\partial x^2} \tag{19}$$

with x being the local coordinate. Eq. (19) can be solved numerically using FDM. For that purpose, the factor $\frac{\partial c_T}{\partial c_L}$ for constant temperature T is derived as

$$\frac{\partial c_T}{\partial c_L} = \frac{KN_T}{N_L\left(K + y_L(1-K)\right)^2} \tag{20}$$

Discretization in time gives for

$$\frac{dc_L}{dt} \approx \frac{\Delta c_L}{\Delta t} = \frac{c_{L,i,j+1} - c_{L,i,j}}{\Delta t} \tag{21}$$

with Δt being the time increment and the indices i and j represent the node number and the number of the time step, respectively. Discretization in space yields

$$\frac{\partial^2 c_L}{\partial x^2} \approx \frac{c_{L,i+1,j+1} - 2c_{L,i,j+1} + c_{L,i-1,j+1}}{\Delta x^2} \tag{22}$$

or

$$\frac{\partial^2 c_L}{\partial r^2} \approx \frac{c_{L,i+1,j+1} - 2c_{L,i,j+1} + c_{L,i-1,j+1}}{\Delta x^2} \tag{23}$$

with Δx being the distance between two neighbouring nodes. Nodes were equidistantly distributed in the models. Dirichlet boundary conditions were prescribed by setting $c_{L,i=0,j} = c_{L,0}$. Inserting the FD formulations into Eq. (19) and resolving for $c_{L,i,j}$ yields an implicit system of equations of the form

$$\boldsymbol{K}\overline{c}_{L,j+1} = \overline{c}_{L,j}. \tag{24}$$

Bold letters $\boldsymbol{K}$ indicate second order tensors. $\overline{c}_{L,j}$ and $\overline{c}_{L,j+1}$ are vectors collecting the nodal lattice concentrations $c_{L,i}$ at the beginning j and the end of the current time increment $j+1$, respectively. The implicit system of equation was solved by computing the inverse of the matrix $\boldsymbol{K}^{-1}$ using an in-house python-based routine. This routine has already been used several times and the interested reader is referenced to previous works of the authors, such as [2,52].

Model description and parametrization

Numerical diffusion models were established to simulate the concentration profiles, effective diffusion coefficients and to evaluate diffusion depths. As illustrated in Fig. 1a, a plane sheet model was used for simulating permeation transients in the presents of trapping sites. Dirichlet boundary conditions were applied on both sides by setting the sub-surface lattice concentrations $c_{L,0}$ and $c_{L,L}$ constant. The boundary condition $c_{L,0}$ at the reduction halve cell side ranged from 10^{-14} to 10^{-6} mol/mm^3, while the boundary condition $c_{L,L}$ was set to zero at the oxidation halve cell side. This causes a gradient of the lattice hydrogen concentration within the plane sheet. The corresponding diffusion flux $j_L|_{x=L}$ was recorded at the oxidation side as a function of sub-surface lattice concentration $c_{L,0}$ and trapping parameters. Under stationary conditions, the lattice concentration profile is linear in the plane sheet and the sub-surface lattice concentration $c_{L,0}$ can be calculated from the stationary flux $j_{L,S}$ using the following equation

$$c_{L,0} = \frac{j_{L,S}}{D_L}L \tag{25}$$

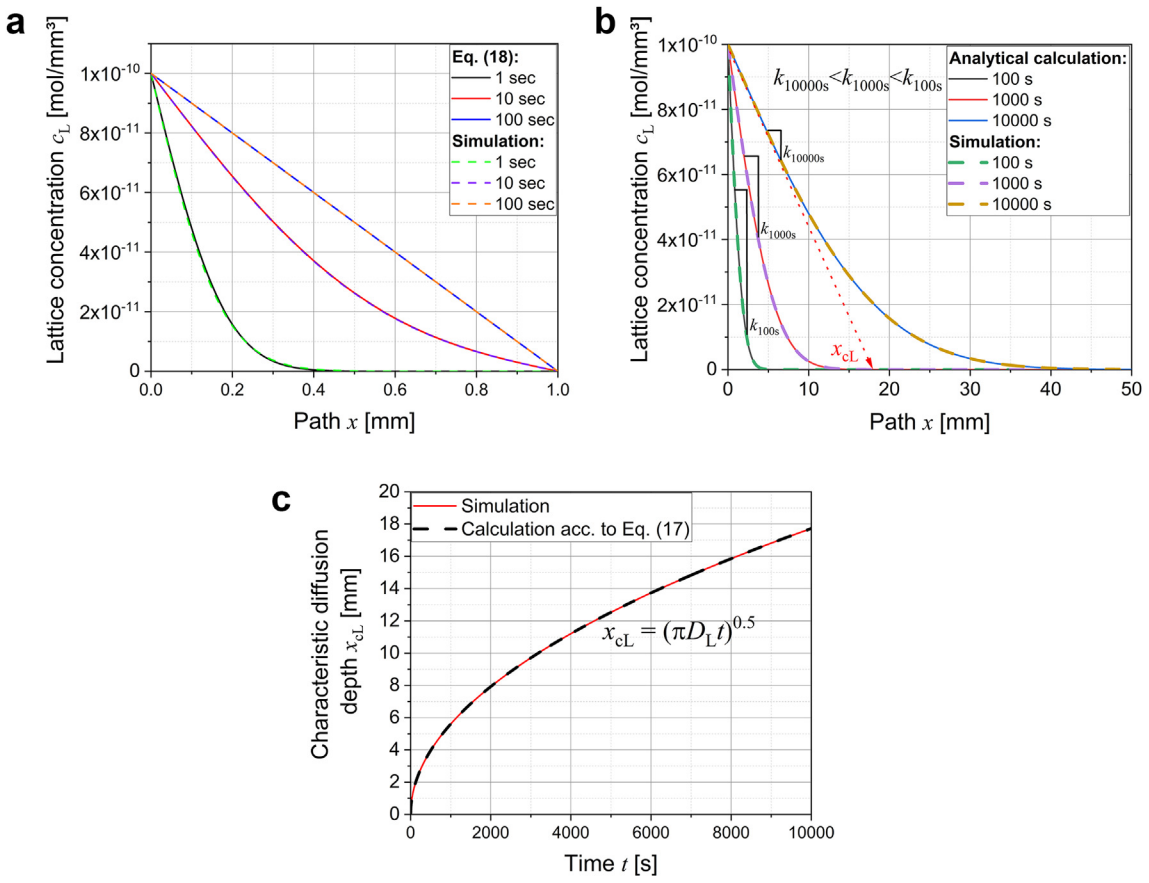

Fig. 2 – a) c_L profile in a plane sheet with $L = 1$ mm. b) c_L profile in a semi-finite volume and c) corresponding characteristic diffusion depth as a function of time.

For a better comparison of the simulated diffusion flux, which is normally given in mol/mm^{2}s, with experiments, a current density i can be calculated by applying Faraday's law as

$$i = j_L F, \tag{26}$$

where F is Faraday constant given as 96485.3329 sA/mol. The sample thickness L was chosen to be 1 mm.

As illustrated in Fig. 1b, the lattice hydrogen concentration profile $c_L(x,t)$ and the characteristic hydrogen diffusion depth $x_c(t)$ in ferritic steels were simulated for a semi-infinite model extending from $x = 0$ to $x = +\infty$. The total simulation time t_{total} was set to 20,000 s, which corresponds to 5.6 h of hydrogen charging. The semi-infinite volume was, different to the others, implemented by choosing a very large thickness compared to the diffusion depth $L = 120\,\text{mm} \gg x$. Furthermore, the sub-surface lattice concentration $c_{L,L}$ at the opposite side was set to zero to guarantee that the hydrogen diffusion into the semi-infinite volume was not affected by any constraint. The characteristic diffusion depth $x_c(t)$ was evaluated as a function of diffusion time t from the simulated total concentration profiles $c(x,t)$ instead of the lattice concentration profile. The shape of the total concentration profile differs significantly from the lattice concentration profile $c_L(x,t)$, by considering also the trapped hydrogen concentration $c_T(x,t)$. The characteristic diffusion depth x_c for a given time is defined as the necessary depth to reach 42% of the sub-surface total concentration $c_0(x = 0)$ as

$$c(x_c, t) = 0.42 \cdot c_0. \tag{27}$$

For studying the role of trapping sites on the effective diffusion coefficient and achievable diffusion depth, three different cases are compared with each other:

- pure ferritic crystals without any trapping sites in the microstructure,
- with shallow trapping sites ($E_b = 30$ kJ/mol) and
- with deep trapping sites ($E_b = 60$ kJ/mol).

For pure crystals, we assumed an interstitial lattice site density N_L of $2 \cdot 10^{-4}$ mm^3/s and a lattice diffusion coefficient D_L of 0.01 mm^2/s, which represent well-annealed ferritic iron [24,25]. A classification into shallow and deep trapping sites is based on the works of Legrand [46]. Therefore, the binding energies of shallow trapping sites and of deep trapping sites were set to 30 kJ/mol and 60 kJ/mol, respectively. While binding energies of 30 kJ/mol are representative for dislocations [62,63] and some grain boundaries [64,65], 60 kJ/mol can be related to titanium of vanadium carbide interfaces [7,8].

Applying Eq. (3) with binding energies above 60 kJ/mol behave quasi-irreversible and lead to remaining TDS peaks even after long lasting vacuum treatments, as it was shown by

Table 1 – Parametrization of the bulk diffusion models.

Model	Parameter and symbol	Value	Unit	Source
General parametrization	Temperature T	20	°C	–
	Lattice diffusion coefficient D_L	0.01	mm^2/s	Assumption made on ferritic iron [25]
	Lattice site density N_L	$2 \cdot 10^{-4}$	mol/mm^3	Assumption made on ferritic iron [41]
	Sub-surface lattice concentration $c_{L,0}$	10^{-9}, 10^{-10}, 10^{-11} or 10^{-12}	mol/mm^3	Assumption made in this work
Pure crystals	Binding energy E_b	0.0	kJ/mol	Assumption made in this work
	Trap density N_T	0.0	mol/mm^3	
Shallow trapping	Binding energy E_b	30	kJ/mol	
	Trap density N_T	10^{-5},10^{-6},10^{-7}, 10^{-8} or 10^{-9}	mol/mm^3	
Deep trapping	Binding energy E_b	60	kJ/mol	
	Trap density N_T	10^{-7}, 10^{-8}, 10^{-9}, 10^{-10} or 10^{-11}	mol/mm^3	

Drexler et al. [7]. Different trap densities N_T of shallow trapping sites were considered in the simulations, as given in Table 1. Based on a previous work of Drexler et al. [24], trap densities in the range from 10^{-9} to 10^{-7} mol/mm^3 correspond to dislocation densities in deformed iron of about 10^{15}, 10^{14} and 10^{12} m/m^3, respectively. The trap density of deep trapping sites was less, as given in Table 1. The lower trap density of deep trapping sites corresponds to the observation that shallow trapping sites are more likely to occur in the microstructure than deep trapping sites [66,67]. Dirichlet boundary conditions were applied by setting the sub-surface lattice concentration $c_{L,0}$ to 10^{-9}, 10^{-10}, 10^{-11} or 10^{-12} mol/mm^3. The total hydrogen concentration at the surface is calculated by using Eqs. (1) and (3) and thus the total hydrogen concentration varies with the chosen trapping parameters E_b and N_T. The initially applied hydrogen concentration in bulk was zero.

Results and discussion

Verification of the FDM implementation was performed using the analytical solutions for lattice hydrogen diffusion in plane sheets and infinite volumes. A comprehensive convergence study was established that the mesh and time increments were adequate to calculate permeation transients and concentration profiles in the presence of trapping sites. Effective diffusion coefficients were simulated as function of sub-surface lattice concentration, sample thickness and trapping parameters. Finally, the diffusion depth was evaluated from simulated total concentration profiles and discussed with respect to validity of the effective diffusion concept.

Verification of the numerical implementation

The implementation of the FDM was checked by comparing with the analytical solutions for plane sheets and semi-infinite volumes, which are given in Eq. (18) and Eq. (14), respectively. In Fig. 2a, simulated lattice concentration profiles $c_L(x,t)$ are presented in a plane sheet model after 1, 10 and 100 s. For pure crystals, the lattice concentration increases rapidly with time and reaches a stationary state after 100 s. The stationary state is characterized by a linear lattice concentration profile and constant flux along the sheet thickness. The numerical solutions are in perfect agreement with the analytical solutions.

In Fig. 2b, simulated lattice concentration profiles $c_L(x,t)$ are given in a semi-infinite volume after 100, 1000 and 10,000 s. With increasing time, hydrogen diffuses from the surface deeper into bulk. This causes a steady decrease of the concentration gradient beneath the surface with increasing diffusion time. The simulated curves agree perfectly well with the analytic expressions for pure crystals. Therefore, also the corresponding characteristic diffusion depths $x_{c_L}(t)$ of the numerical and analytical solutions are in perfect agreement, as shown in Fig. 2c. For both solutions, the characteristic diffusion depth $x_{c_L}(t)$ increases with the square root of the diffusion time t and of the effective diffusion coefficient $D_{eff} = D_L$. The square root dependency relates to the decrease in the concentration gradient with time.

Convergence study

In modelling, it is always difficult to choose automatically the time increment and node density that ensures convergence of the simulation results. For that purpose, a convergence study was established that allows to use of adequate time increments and node densities with respect to the chosen trapping parameters.

Fig. 3a shows permeation transients simulated for pure crystals as a function of time increment dt. 100 nodes were considered for a sheet thickness L of 1 mm. With decreasing time increment the permeation transients become smoother and converge with a time increment of 0.1 s to a sigmoidal shaped curve with a timelag t_{lag} of 16.67 s. As shown in Fig. 3b, this corresponds to an effective diffusion coefficient of 0.010 mm^2/s. The relative error with respect to the exact solution D_L was less than 2% and choosing lower time increments does not improve the accuracy significantly. Furthermore, increasing the number of nodes from 10 to 1000 affected the simulation results and thus the accuracy only minor. For pure crystals without trapping sites, a node density of 0.01 mm^{-1} and a time increment of 0.1 s are suggested to ensure convergence of the numerical simulations.

Studying the influence of the chosen time increment dt and node distance dx on the simulated permeation transients of real crystals with trapping sites, revealed a strong correlation between accuracy of the effective diffusion coefficient and the chosen binding energy. Basically, with increasing binding energy, the time increment needs to be smaller and also the node density has to be increased. Fig. 3c and d shows the simulated effective diffusion coefficients for shallow trapping and deep trapping, respectively, as a function of inverse time increment and number of nodes. Based on the present results, a minimum

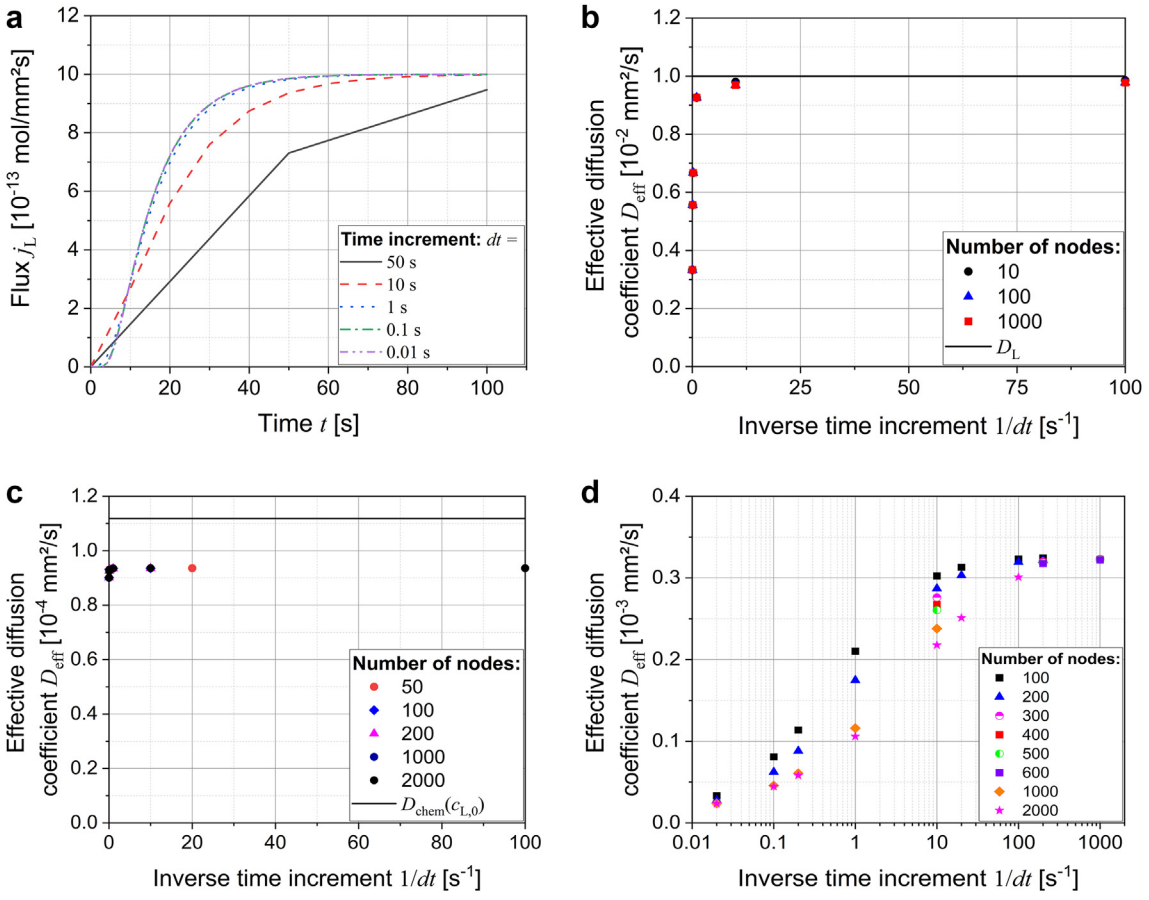

Fig. 3 – a) Permeation transients for pure crystals as a function of *dt* for a given node density of 0.01 mm^{-1}. Time and mesh convergence study to simulate the effective diffusion coefficients: b) pure crystals, c) shallow trapping with $N_T = 10^{-7}$ mol/mm^3 and d) deep trapping with $N_T = 10^{-9}$ mol/mm^3.

time increment of 0.1 s and a node density of 0.005 mm $^{-1}$ are suggested for shallow trapping, while a minimum time increment of 0.005 and a node density of 0.003 have to be applied for deep trapping. Table 2 summarizes the necessary discretization parameters to ensure adequate numerical solutions of permeation transients and effective diffusion coefficients for pure crystals and in the presence of trapping sites.

The numerical parameters, which were found for the plane sheet model, were also checked for the semi-infinite volume model. For that purpose, the influence of the chosen time increment *dt* was studied on the simulated lattice concentration profiles in the presence of shallow and deep trapping sites, as shown in Fig. 4a and b, respectively. The node density was 0.003 mm^{-1}. In case of shallow trapping sites with a trap density of 10^{-7} mol/mm^3 the lattice concentration decreases almost parabolically, while deep trapping sites with a trap density of 10^{-9} mol/mm^3 cause a linear decrease of the lattice concentration from the surface into the volume. The numerical parameters necessary to reach time and mesh convergence are equal in the plane sheet model and the semi-infinite volume model.

Table 2 – Necessary discretization parameters to reach convergence of D_{eff}.

Model parametrization	Min. time increment [s]	Node density [mm^{-1}]	Residual error *E*
Pure crystal	0.1	0.01	<2%
Shallow trapping	0.1	0.005	
Deep trapping	0.05	0.003	

Effective diffusion coefficient D_{eff}

Fig. 5a and b shows representative permeation transients simulated for shallow trapping sites with a trap density of 10^{-7} mol/mm^3 and deep trapping sites with a trap density of 10^{-9} mol/mm^3, respectively. The shapes of the recorded permeation transients change from a sigmoidal to almost a step function course with increasing binding energy. The sub-surface lattice concentration $c_{L,0}$ increases the stationary flux $j_{L,S}$ according to Eq. (26) and shifts the permeation transients to shorter times. For a better comparability of the time shift with respect to the lattice concentration, the corresponding normalized permeation transients are shown in Fig. 5c and d. Hence, an increase in the sub-surface lattice concentration on the reduction halve cell side causes a decrease in the timelag for given trapping parameters.

The effective diffusion coefficients were evaluated from the simulated permeation transients, according to Eq. (11). The effect of the sub-surface lattice concentration on the

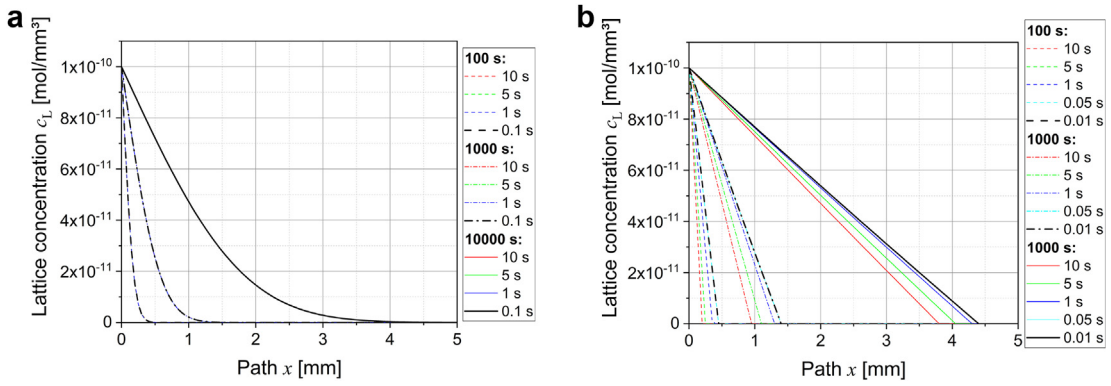

Fig. 4 – Time convergence study for semi-infinite volumes with $c_{L,0} = 10^{-10}$ mol/mm³: a) shallow trapping with $N_T = 10^{-7}$ mol/mm³ and b) deep trapping with $N_T = 10^{-7}$ mol/mm³.

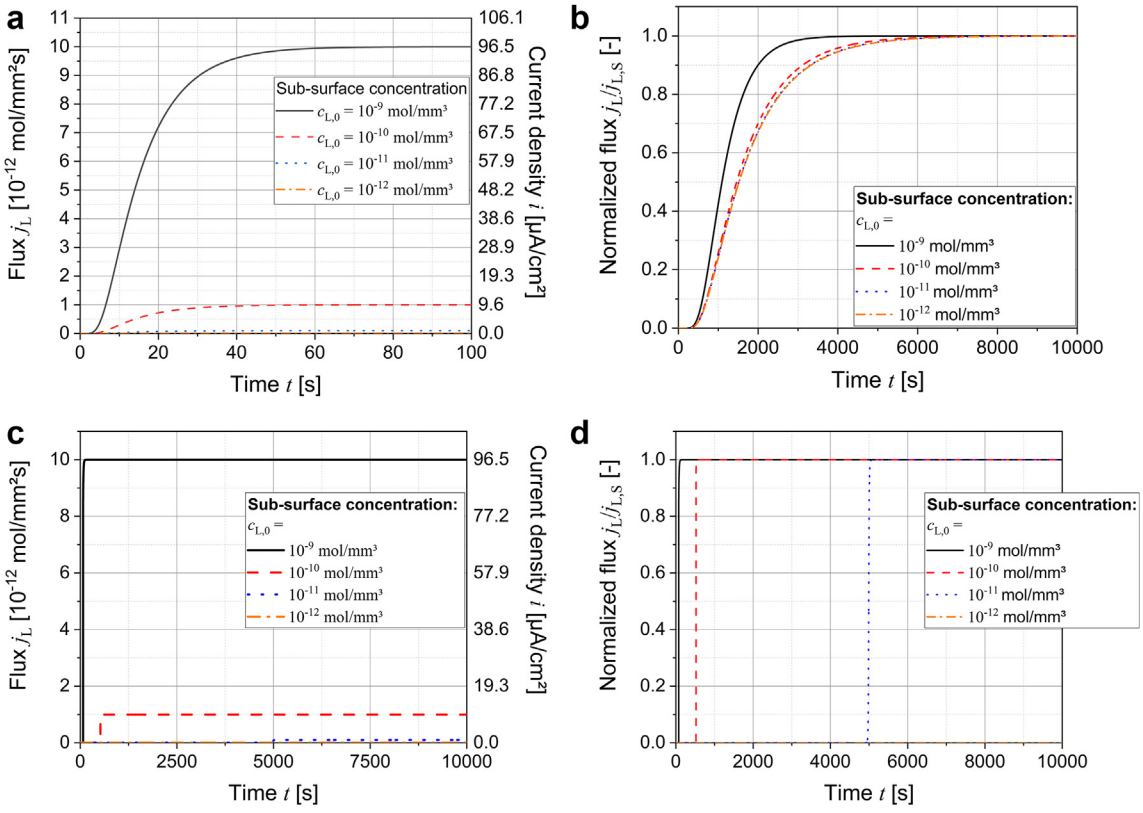

Fig. 5 – Influence of $c_{L,0}$ on simulated permeation transients: a) shallow trapping with $N_T = 10^{-7}$ mol/mm³ and b) deep trapping with $N_T = 10^{-9}$ mol/mm³. The corresponding normalized permeation transients are shown in c) and d), respectively.

effective diffusion coefficient is shown in Fig. 6. Apparently, the effective diffusion coefficients depend not only on the binding energy and trap density, but also on the sub-surface lattice concentration. Obviously, the effective diffusion coefficient becomes constant at very low or very high lattice concentrations. The maximum of the effective diffusion coefficient at high lattice concentrations equals the lattice diffusion coefficient $D_{eff} = D_L$. However, to reach the maximum in the lattice-diffusion controlled regime a minimum sub-surface lattice concentration of 10^{-9} mol/mm³ would be necessary. According to Eq. (26), this corresponds to a current density of 97.5 μA/cm², which is much larger than typical stationary current densities measured in literature by electrochemical permeation ranging between 1 and 25 μA/cm² [68]. In other words, even with this highest current density the real lattice hydrogen diffusion coefficient of 0.01 mm²/s cannot be evaluated from simulated permeation transients.

The effective diffusion concept was criticised in literature to be in contradiction to the concept of chemical bulk diffusion [38]. To that purpose, the corresponding chemical diffusion

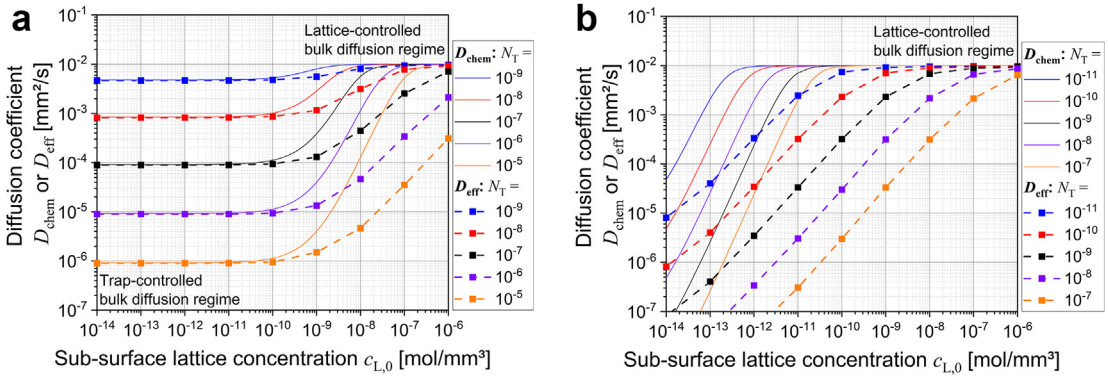

Fig. 6 – D_{chem} compared with D_{eff} as function of $c_{L,0}$: a) shallow trapping and b) deep trapping.

coefficients for shallow and deep trapping sites were added to Fig. 6a and b, respectively. For simplification the chemical diffusion coefficient was calculated for the sub-surface lattice concentration $c_{L,0}$ at the reduction halve cell side according to Eq. (11) taking account Eq. (20). The maximum of the chemical diffusion coefficient is always limited by the lattice diffusion coefficient D_L, which was set to 0.01 mm^2/s. That value corresponds to hydrogen bulk diffusion, when all the trapping sites have been completely filled and the trap site fraction is $y_T = 1$. The minimum of the chemical diffusion coefficient is magnitudes lower and corresponds to the trap-controlled bulk diffusion regime. For intermediate lattice concentrations, the effective diffusion coefficients underestimate the chemical diffusion coefficients and the difference between the chemical diffusion coefficient and the effective diffusion coefficient is greater for deep trapping sites than for shallow trapping sites. Anyway, a qualitative agreement for single trapping sites was observed between the simulated effective diffusion coefficients and the concentration dependency of chemical diffusion coefficient. However, this presupposes that the effective diffusion coefficient is measured or simulated as function of the sub-surface lattice concentration.

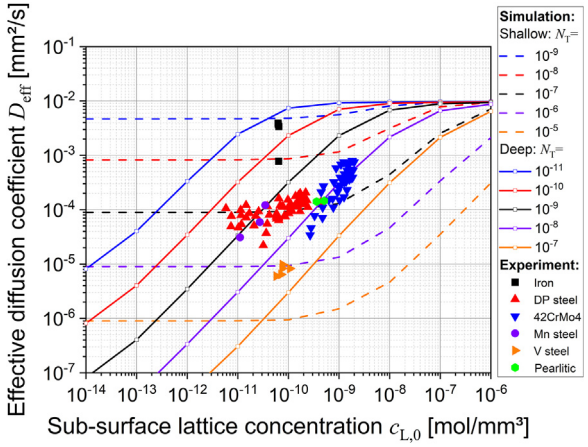

Fig. 7 – Concentration dependency of simulated and measured effective diffusion coefficients: iron [25], dual phase steels [69–71], 42CrMo4 [26], Low carbon Mn steels [72], High carbon V steels [73] and pearlitic steels [38].

In Fig. 7, measured effective diffusion coefficients for different materials and heat treatments were collected as function of sub-surface lattice concentration from literature. The corresponding sub-surface lattice concentration $c_{L,0}$ was calculated from the measured stationary flux $j_{L,S}$ using Eq. (25). Hence, only those literature values could be used, which provide full information of the measured data, especially the thickness and the value of stationary flux. Furthermore, the thicknesses of the measured values were all around 1 mm and thus comparable with the thickness used in the plane sheet model. Obviously, the measured effective diffusion coefficients follow an increasing trend with the sub-surface lattice concentration. This concentration dependency of the effective diffusion coefficient is a clear indication of the influence of trapping sites on hydrogen diffusion in steels. Hence, it is recommended that the effective diffusion coefficient should always be measured as function of lattice concentration instead of performing single measurements. For example, Zafra et al. [26] demonstrated experimentally that this is possible by using the permeation technique employing the stepped build-up transient procedure.

Due to the concentration dependency of simulated permeation transients, also the influence of the sheet thickness L on the effective diffusion coefficient was studied numerically, shown in Fig. 8a and b. Typical sample thicknesses used to measure the effective diffusion coefficients in literature range from 0.5 to 2 mm [20,70,74]. Obviously, a sheet thickness of more than 1 mm, lead to unaffected effective diffusion coefficients. However, with smaller sheet thicknesses $L < 1$ mm a slight decrease was observed of the simulated effective diffusion coefficients.

The basic assumption of space and time independency of the effective diffusion concept can be verified by replacing $\partial c_T / \partial c_L$ in Eq. (11) with Eq. (20). This allows to calculate the thermodynamic factor $1/(1+\partial c_T/\partial c_L)$ as function of lattice concentration for shallow and deep trapping sites, as shown in Fig. 9a and b, respectively. In both trapping scenarios the thermodynamic factor depends on the local lattice concentration. Since the lattice concentration decreases through the thickness (cf. Fig. 2a) and increases steadily during the permeation test, the space and time independency are never given. This would also agree with the measured effective diffusion coefficients found in literature, which follow an

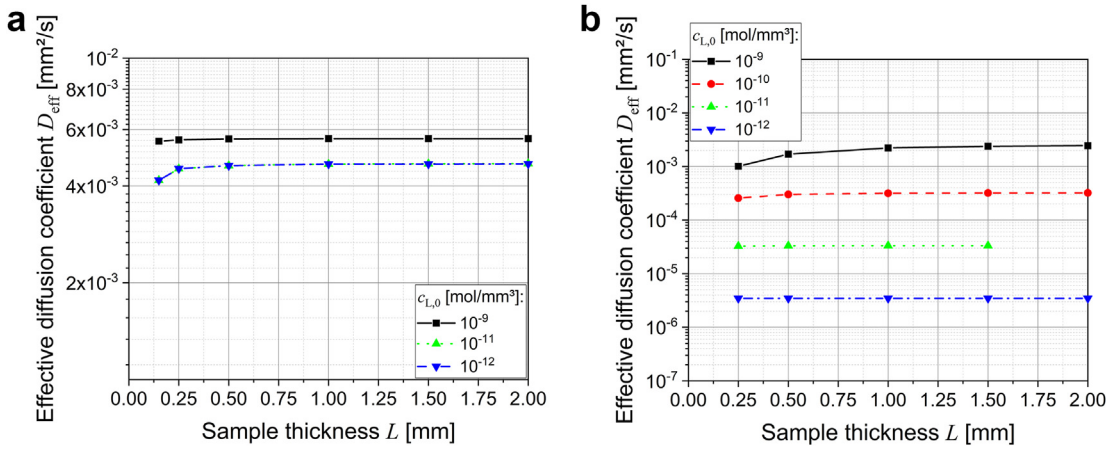

Fig. 8 – Thickness dependency of D_{eff}: a) shallow trapping and b) deep trapping both with $N_T = 10^{-9}$ mol/mm³.

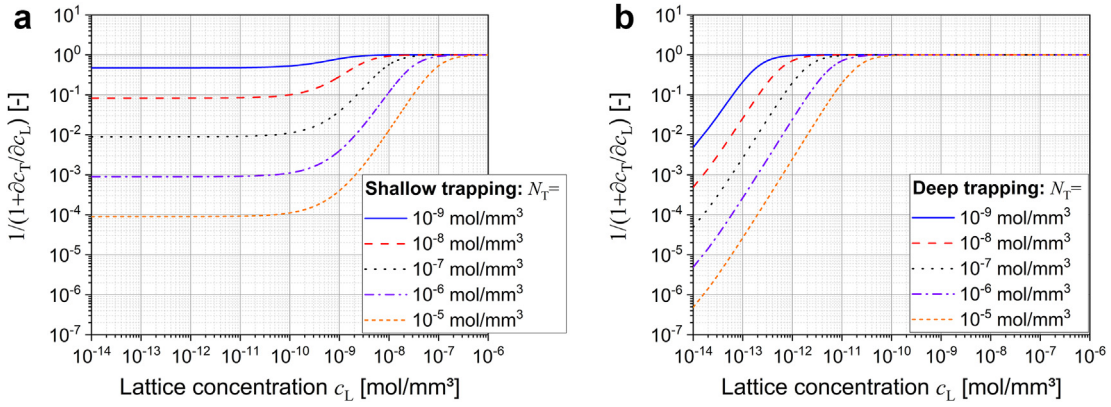

Fig. 9 – Concentration dependency of the factor $1/(1+\partial c_T/\partial c_L)$: a) shallow trapping sites and b) deep trapping sites.

increasing trend with increasing sub-surface lattice concentration (cf. Fig. 7).

Generally, the basic assumption of space and time independency of the effective diffusion coefficient seems to be violated in many experimental situations. Therefore, the concept of effective diffusion is not physically based and simulations of the hydrogen distributions using Eq. (10) must be treated with utmost care. Anyway, the effective diffusion coefficient can be treated as a semi-empirical measure of the chemical diffusion coefficient. For this, the effective diffusion coefficient must be measured as function of sub-surface lattice concentration. Based on the present observation, it is strongly recommended to always plot measured effective diffusion coefficients as function of sub-surface lattice concentrations, as done in Fig. 7, instead of comparing single values.

Characteristic diffusion depth x_c

As the basic assumption of a space and time independency of the effective diffusion coefficient is not fulfilled, also the square root dependency of the diffusion depth with the effective diffusion coefficient and time needs additional attention. For that purpose, three different microstructural scenarios were considered to study the effect of microstructural trapping sites on the evolution of the characteristic diffusion depth in the semi-infinite volume model:

- pure crystals without hydrogen trapping sites,
- with shallow hydrogen trapping sites and
- with deep hydrogen trapping sites.

The trap densities N_T were varied to intensify the effect of the hydrogen trapping on the long-range chemical diffusion. During bulk diffusion, trapping sites are progressively filled from the surface side into bulk. Assuming that the kinetics of hydrogen motion are governed by diffusion through the crystal lattice, trapping sites retard chemical diffusion and reduce the characteristic diffusion depth with respect to pure crystals. The influence of the hydrogen ingress by varying the sub-surface lattice concentration was considered as well in the present investigations.

Fig. 10 shows simulated profiles of the total hydrogen concentration c and corresponding trapped hydrogen concentration c_T as a function of time. The corresponding lattice concentration profiles were shown earlier in Fig. 4. The lattice hydrogen concentration is only a small part of the total concentration and most of the hydrogen is trapped at microstructural defect sites. Therefore, the characteristic

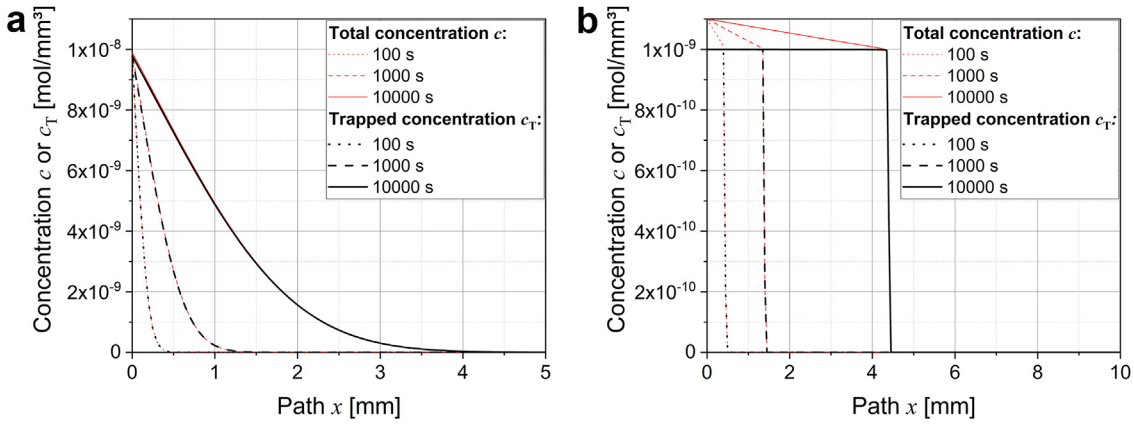

Fig. 10 – c and c_T profiles in a semi-infinite volume considering a) shallow trapping sites with $N_T = 10^{-7}$ mol/mm³ and b) deep trapping sites with $N_T = 10^{-9}$ mol/mm³.

diffusion depth is in the presence of trapping sites related to the total hydrogen concentration profile instead to the lattice concentration profile. The trap site fraction y_T correlates with the binding energy and becomes almost one above 60 kJ/mol. The larger trap concentration c_T in the presence of shallow trapping sites instead of deep trapping sites results from the larger trap densities of 10^{-7} mol/mm³ compared to 10^{-9} mol/mm³. As shown in Fig. 10a and b, trapping sites have two effects:

1. the shape of the concentration profile changes from smooth to an almost step function like course.
2. With increasing binding energy and trap density, the diffusion depth is drastically reduced compared to pure crystals (cf. Fig. 2c).

Fig. 11 shows the evolution of the squared characteristic diffusion depth x_c^2 as a function of time considering shallow trapping sites and deep trapping sites. The step-like course relates to diffusion and the discretization in space. Only two of four considered hydrogen charging scenarios are shown in Fig. 11, namely a lattice concentration of 10^{-12} and 10^{-9} mol/mm³. The characteristic diffusion depth was related to the total hydrogen concentration and not to the lattice hydrogen concentration profile. Although, the trap density decreased the characteristic diffusion depth significantly, microstructural trapping sites do not change the linearity of the characteristic diffusion depth with the square root of time $x_c \sim \sqrt{t}$.

In addition, the role of hydrogen charging was simulated by altering the sub-surface lattice concentration from 10^{-12} to 10^{-9} mol/mm³. As shown in Fig. 11a, trapping causes a concentration dependency of the chemical diffusion coefficient $D_{chem}(c)$ and thus, a decrease of the sub-surface lattice concentration also decreases the chemical diffusivity (cf. Fig. 6). At the first glance, this trend is also visible in the simulated characteristic diffusion depth:

- the effect of shallow trapping sites is shown in Fig. 11a and b. A sub-surface lattice concentration of 10^{-12} mol/mm³ and a trap density of 10^{-7} mol/mm³ (bold blue line) resulted in a diffusion depth of 1.55 mm after 20,000 s, while an increase of the sub-surface concentration to 10^{-9} mol/mm³ increased the diffusion depth to 2.65 mm after 20,000 s.
- The effect of deep trapping sites is shown in Fig. 11c and d. An increase of the sub-surface concentration of 10^{-12} to 10^{-9} mol/mm³ results for a trap density of 10^{-9} mol/mm³ (bold blue line) in an increase of the characteristic diffusion depth from 0.65 to 16 mm.

Additional attention has to be drawn to the simulation results shown in Fig. 11d. Due the high sub-surface lattice concentration of 10^{-9} mol/mm³ and the deep trapping sites with $y_T = 1$, the chemical diffusion coefficient is equal the lattice diffusion coefficient $D_{chem} = D_L$ (cf. Fig. 6b) and thus, the diffusion depth is insensitive to hydrogen trapping. Hydrogen diffusion in this concentration range is named lattice diffusion-controlled throughout this work.

Hydrogen diffusion in pure crystals without trapping sites, follows classical Fick's law with the highest possible characteristic diffusion depth for hydrogen of 16 mm after 20,000 s and no concentration dependency was observed. While in the presence of trapping sites a correlation of the characteristic diffusion depth with the square root of time is physical based, a dependency on the effective diffusion coefficient does not seem apparent. According to Eq. (27), a constant pre-factor $\sqrt{nD_{eff}}$ can be applied for pure crystals with the scale factor $n = 1.26$ independent of the applied sub-surface concentration. As shown in Fig. 11, linear fitting of $x_c = \sqrt{nD_{eff}t}$ to the simulated curves, revealed scale factors n ranging from 1.30 to 6.04. Thus, in the presence of trapping sites and dependent on the sub-surface lattice concentration, the scale factor is not a constant anymore. Obviously, in case of deep trapping the scale factors are much larger than in the case of shallow trapping. This difference can be explained by the difference between the chemical diffusion coefficient and the corresponding effective diffusion coefficient, as shown in Fig. 6. The greater the difference the larger is the scale factor n.

Using the well-known correlation $x_c = \sqrt{nD_{eff}t}$ for experimental analysis for given materials, as outlined in the introduction, it is strongly recommended to choose the scale factor

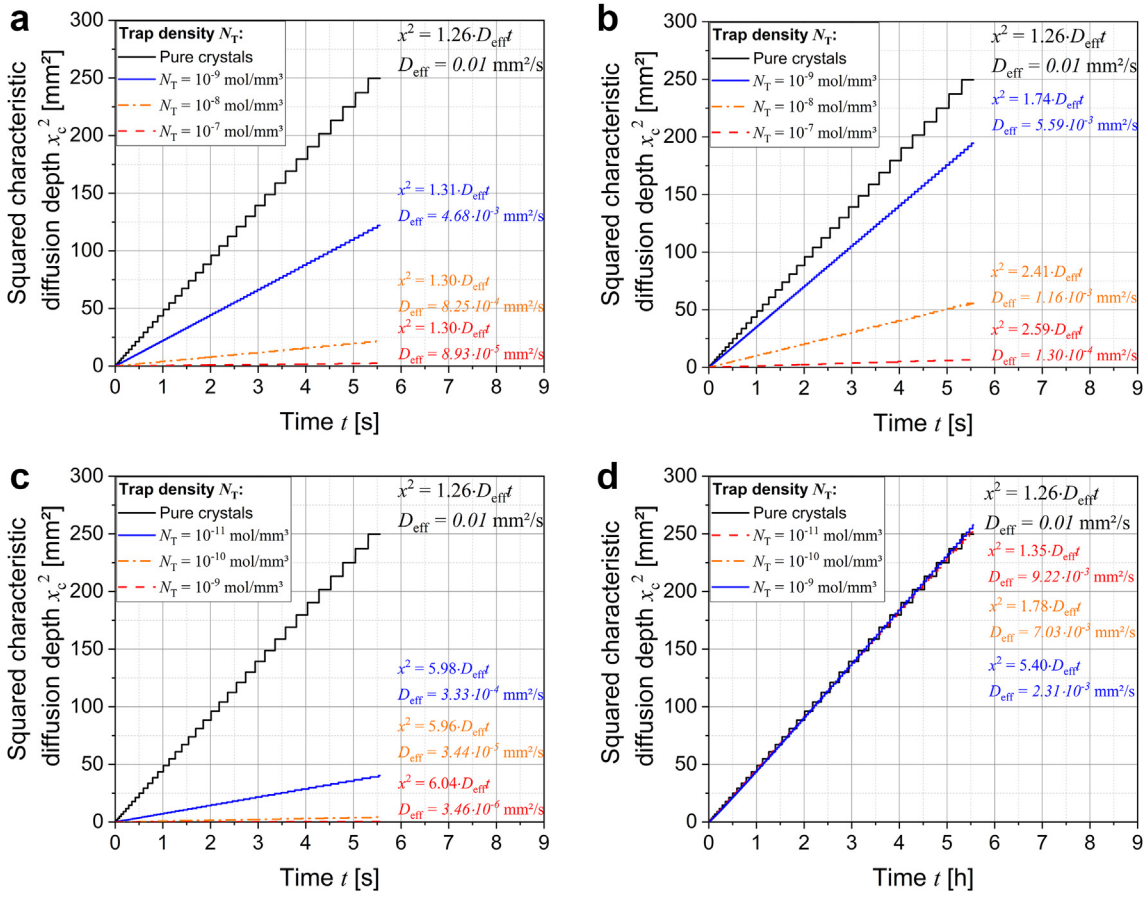

Fig. 11 – Representative $x_c^2(t)$ for shallow trapping sites with $c_{L,0}$ of a) 10^{-12} and b) 10^{-9} mol/mm³ and for deep trapping sites with $c_{L,0}$ of c) 10^{-12} and d) 10^{-9} mol/mm³.

n wisely. According to the theoretical results from the present work,

- the real characteristic diffusion depth may be underestimated by a factor of six or
- the real hydrogen charging time $t = x_c^2/nD_{eff}$ could be chosen shorter and much more efficient.

Conclusions

Based on the bulk diffusion theory the effective diffusion concept was critically discussed. Permeation transients $j_L(t)$ and diffusion depth profiles $c(x,t)$ were simulated for shallow and deep trapping sites by numerically solving the generalized bulk diffusion equation. To guarantee adequate solutions, the implementation of the FDM was checked with analytical solutions and a comprehensive convergence study was performed. Evaluations of the effective diffusion coefficients D_{eff} and characteristic diffusion depths x_c revealed the following conclusions:

- the basic assumption of space and time independency of the effective diffusion coefficient fails in a broad concentration range. This leads to pronounced concentration dependency of the effective diffusion coefficient.
- The effective diffusion coefficient cannot be regarded as a material constant. Therefore, the constant effective diffusion coefficient should not be used for diffusion simulations.
- A correlation of the characteristic diffusion depth x_c with the square root of the effective diffusion coefficient $\sqrt{D_{eff}}$ was not found. Nevertheless, progressively filling of microstructural trapping sites from the surface into bulk does not alter the well-known square root dependency of the characteristic diffusion depth $x_c \sim \sqrt{t}$ on time.
- Although the effective diffusion concept is not physical based, the effective diffusion coefficient was found to qualitatively correlate with the concentration dependent chemical diffusion coefficient.
- Effective diffusion coefficients should be measured as function of sub-surface lattice concentration using the permeation technique, for example, employing the stepped build-up transient procedure. For comparing measured effective diffusion coefficients resulting from different materials or heat treatments, the effective diffusion coefficients should be plotted as function of the sub-surface lattice concentration, like shown in Fig. 7.

- Based on the present results, a revision of the corresponding ASTM and EN ISO standards for electrochemical permeation measurements is recommended.

Declaration of competing interest

The authors declare that they have no known competing financial interests or personal relationships that could have appeared to influence the work reported in this paper.

Acknowledgement

The Comet Centre CEST is funded within the framework of COMET – Competence Centres for Excellent Technologies by BMVIT, BMDW as well as the Province of Lower Austria and Upper Austria. The COMET programme is run by FFG (FFG 865864 CEST-K1).

List of symbols

c	Total hydrogen concentration [mol/mm^3]
c_0	Sub-surface total hydrogen concentration [mol/mm^3]
c_L	Lattice hydrogen concentration [mol/mm^3]
$c_{L,0}$	Lattice boundary condition at $x = 0$ mm [mol/mm^3]
$c_{L,L}$	Lattice boundary condition at $x = L$ [mol/mm^3]
c_T	Trap hydrogen concentration [mol/mm^3]
D_0	Jump frequency [mm^2/s]
D_{chem}	Chemical diffusion coefficient [mm^2/s]
D_{eff}	Effective diffusion coefficient [mm^2/s]
D_L	Lattice diffusion coefficient [mm^2/s]
D_T	Trap diffusion coefficient [mm^2/s]
E	Residual error [–]
E_b	Binding energy [kJ/mol]
E_m	Migration energy of lattice hydrogen [kJ/mol]
$E_{m,T}$	Migration energy of trapped hydrogen [kJ/mol]
F	Faraday constant [As/mol]
i	Current density [μA/cm^2]
j_L	Hydrogen lattice flux [mol/mm^{2}s]
$j_{L,S}$	Stationary diffusion flux [mol/mm^{2}s]
K	Equilibrium constant [–]
L	Sheet thickness [mm]
N_L	Lattice site density [mol/mm^3]
N_T	Trap density [mol/mm^3]
n	Scale factor [–]
n_D	Timelag factor [–]
R_g	Universal gas constant [J/Kmol]
T	Temperature [K]
t	Time [s]
t_{lag}	Timelag [s]
t_{total}	Total simulation time [s]
dt	Time increment [s]
v	Diffusion speed [mm^2/s]
x	Local coordinate [mm]
x_c	Characteristic diffusion depth [mm]
dx	Node distance [mm]
y_L	Lattice site fraction [–]
y_T	Trap site fraction [–]

List of abbreviations

DP	Dual phase
FD	Finite difference
FDM	Finite difference method
HAC	Hydrogen assisted cracking
HE	Hydrogen embrittlement
TDA	Thermal desorption analysis
TDS	Thermal desorption spectroscopy

REFERENCES

[1] Elsayed H, Drexler A, Warchomicka F, Traxler I, Domitner J, Galler M, Vallant R. Resistance of quench and partitioned steels against hydrogen embrittlement. J Mater Eng Perform 2022. https://doi.org/10.1007/s11665-022-07438-4.

[2] Drexler A, Helic B, Silvayeh Z, Mraczek K, Sommitsch C, Domitner J. The role of hydrogen diffusion, trapping and desorption in dual phase steels. J Mater Sci 2022;57:4789–805. https://doi.org/10.1007/s10853-021-06830-0.

[3] Cao JL, Li LT, Wu JX, Lu YP, Gui ZL. Diffusion of hydrogen in a steel substrate absorbed during zinc and zinc-silica electroplating. Corrosion 2002;58:698–702. https://doi.org/10.5006/1.3287700.

[4] Mandy M, Nabi B, Larnicol M, Vanden Eynde X, Georges C, Goodwin F. Influence of Zn-based coating alloys on hydrogen diffusion and corrosion resistance in a DP steel. BHM Berg-Hüttenmännische Monatsh 2021. https://doi.org/10.1007/s00501-021-01160-9.

[5] Hillier EMK, Robinson MJ. Hydrogen embrittlement of high strength steel electroplated with zinc-cobalt alloys. Corrosion Sci 2004;46:715–27. https://doi.org/10.1016/S0010-938X(03)00180-X.

[6] Laureys A, Claeys L, De Seranno T, Depover T, Van den Eeckhout E, Petrov R, Verbeken K. The role of titanium and vanadium based precipitates on hydrogen induced degradation of ferritic materials. Mater Char 2018;144:22–34. https://doi.org/10.1016/j.matchar.2018.06.030.

[7] Drexler A, Depover T, Leitner S, Verbeken K, Ecker W. Microstructural based hydrogen diffusion and trapping models applied to Fe-C X alloys. J Alloys Compd 2020;826:154057. https://doi.org/10.1016/j.jallcom.2020.154057.

[8] Drexler A, Depover T, Verbeken K, Ecker W. Model-based interpretation of thermal desorption spectra of Fe-C-Ti alloys. J Alloys Compd 2019;789:647–57. https://doi.org/10.1016/j.jallcom.2019.03.102.

[9] Drexler A, Domitner J, Sommitsch C. Modeling of hydrogen diffusion in slow strain rate (SSR) testing of notched samples. 143rd ed. Springer Nature Switzerland AG; 2021. https://doi.org/10.1007/978-3-030-66948-5_6.

[10] Polyanskiy VA, Belyaev AK, Alekseeva EL, Polyanskiy AM, Tretyakov DA, Yakovlev YA. Phenomenon of skin effect in metals due to hydrogen absorption. Continuum Mech Therm 2019;31:1961–75. https://doi.org/10.1007/s00161-019-00839-2.

[11] Polyanskiy VA, Belyaev AK, Chevrychkina AA, Varshavchik EA, Yakovlev YuA. Impact of skin effect of hydrogen charging on the Choo-Lee plot for cylindrical samples. Int J Hydrogen Energy 2021;46:6979–91. https://doi.org/10.1016/j.ijhydene.2020.11.192.

[12] Drexler A, He S, Pippan R, Romaner L, Razumovskiy VI, Ecker W. Hydrogen segregation near a crack tip in nickel. Scripta Mater 2021;194:113697. https://doi.org/10.1016/j.scriptamat.2020.113697.

[13] Drexler A, He S, Razumovskiy V, Romaner L, Ecker W, Pippan R. Verification of the generalised chemical potential for stress-driven hydrogen diffusion in nickel. Phil Mag Lett 2020;100:513–23. https://doi.org/10.1080/09500839.2020.1808253.
[14] Massone A, Manhard A, Drexler A, Posch C, Ecker W, Maier-Kiener V, Kiener D. Addressing H-material interaction in fast diffusion materials-A feasibility study on a complex phase steel. Materials 2020;13:4677. https://doi.org/10.3390/ma13204677.
[15] Drexler A, Konert F, Sobol O, Rhode M, Domitner J, Sommitsch C, Böllinghaus T. Enhanced gaseous hydrogen solubility in ferritic and martensitic steels at low temperatures. Int J Hydrogen Energy 2022;47:39639–53. https://doi.org/10.1016/j.ijhydene.2022.09.109.
[16] Wipf H. Solubility and diffusion of hydrogen in pure metals and alloys. Phys Scripta 2001;T94:43. https://doi.org/10.1238/Physica.Topical.094a00043.
[17] Drexler A, Ecker W, Winzer N, Mraczek K, Kokotin V, Manke G, Bergmann C. A step towards numerical evaluation of the local hydrogen susceptibility of punched and cold-formed advanced high strength steel (AHSS) sheets. In: Duprez L, editor. Steely Hydrogen, ocas; 2018. A02. http://steelyhydrogen2018proc.be/articles/pdf/2.
[18] Drexler A, Bergmann C, Manke G, Kokotin V, Mraczek K, Leitner S, Pohl M, Ecker W. Local hydrogen accumulation after cold forming and heat treatment in punched advanced high strength steel sheets. J Alloys Compd 2021;856:158226. https://doi.org/10.1016/j.jallcom.2020.158226.
[19] Drexler A, Helic B, Silvayeh Z, Sommitsch C, Mraczek K, Domitner J. Influence of plastic deformation on the hydrogen embrittlement susceptibility of dual phase steels. Key Eng Mater 2022;926:2077–91. https://doi.org/10.4028/p-oeev6l.
[20] Zafra A, Harris Z, Sun C, Martínez-Pañeda E. Comparison of hydrogen diffusivities measured by electrochemical permeation and temperature-programmed desorption in cold-rolled pure iron. J Nat Gas Sci Eng 2021;98:104365. https://doi.org/10.1016/j.jngse.2021.104365.
[21] Montupet-Leblond F, Hodille EA, Payet M, Delaporte-Mathurin R, Bernard E, Charles Y, Mougenot J, Vartanian S, Grisolia C. Influence of traps reversibility on hydrogen permeation and retention in Eurofer97. Nucl Fusion 2022;62. https://doi.org/10.1088/1741-4326/ac6e74.
[22] Toribio J, Kharin V. A generalised model of hydrogen diffusion in metals with multiple trap types. Philos Mag 2015;95:3429–51. https://doi.org/10.1080/14786435.2015.1079660.
[23] Kirchheim R. Bulk diffusion-controlled thermal desorption spectroscopy with examples for hydrogen in iron. Metall. Mater. Trans. A Phys. Metall. Mater. Sci. 2016;47:672–96. https://doi.org/10.1007/s11661-015-3236-2.
[24] Drexler A, Siegl W, Ecker W, Tkadletz M, Klösch G, Schnideritsch H, Mori G, Svoboda J, Fischer FD. Cycled hydrogen permeation through Armco iron - a joint experimental and modeling approach. Corrosion Sci 2020;176:109017. https://doi.org/10.1016/j.corsci.2020.109017.
[25] Siegl W, Ecker W, Klarner J, Kloesch G, Mori G, Drexler A, Winter G, Schnideritsch H. Hydrogen trapping in heat treated and deformed Armco iron. In: NACE - int. Corros. Conf. Ser; 2019. p. 1–12.
[26] Zafra A, Peral LB, Belzunce J. Hydrogen diffusion and trapping in A 42CrMo4 quenched and tempered steel: influence of tempering temperature. Int J Hydrogen Energy 2020;45:31225–42. https://doi.org/10.1016/j.ijhydene.2020.08.134.
[27] Zafra A, Belzunce J, Rodríguez C. Hydrogen diffusion and trapping in 42CrMo4 quenched and tempered steel: influence of quenching temperature and plastic deformation. Mater Chem Phys 2020;255:123599. https://doi.org/10.1016/j.matchemphys.2020.123599.
[28] Devanathan MAV, Stachurski Z. The adsorption and diffusion of electrolytic hydrogen in palladium. Proc. R. Soc. London. Ser. A. Math. Phys. Sci. 1962;270:90–102. https://doi.org/10.1098/rspa.1962.0205.
[29] Darken LS, Smith RP. Behavior of hydrogen in steel during and after immersion in acid. Corrosion 1949;5:1–16. https://doi.org/10.5006/0010-9312-5.1.1.
[30] ASTM. ASTM G148-197(2018): standard practice for evaluation of hydrogen uptake, permeation, and transport in metals by an electrochemical technique. 2018.
[31] ISO. DIN EN ISO 17081:2014-10, Elektrochemisches Verfahren zur Messung der Wasserstoffpermeation und zur Bestimmung von Wasserstoffaufnahme und -transport in Metallen. 2014 [n.d.)].
[32] Depover T, Wallaert E, Verbeken K. Fractographic analysis of the role of hydrogen diffusion on the hydrogen embrittlement susceptibility of DP steel. Mater Sci Eng 2016;649:201–8. https://doi.org/10.1016/j.msea.2015.09.124.
[33] Depover T, Wallaert E, Verbeken K. On the synergy of diffusible hydrogen content and hydrogen diffusivity in the mechanical degradation of laboratory cast Fe-C alloys. Mater Sci Eng 2016;664:195–205. https://doi.org/10.1016/j.msea.2016.03.107.
[34] Depover T, Van den Eeckhout E, Verbeken K. The impact of hydrogen on the ductility loss of bainitic Fe-C alloys. Mater Sci Technol 2016;32:1625–31. https://doi.org/10.1080/02670836.2015.1137387.
[35] Zafra A, Belzunce J, Rodríguez C, Fernández-Pariente I. Hydrogen embrittlement of the coarse grain heat affected zone of a quenched and tempered 42CrMo4 steel. Int J Hydrogen Energy 2020;45:16890–908. https://doi.org/10.1016/j.ijhydene.2020.04.097.
[36] W. G., Y. Y., L. J., H. J., S. Y., Q. L.. Hydrogen embrittlement assessment of ultra-high strength steel 30CrMnSiNi2. Corrosion Sci 2013;77:273–80.
[37] Koyama M, Tasan CC, Akiyama E, Tsuzaki K, Raabe D. Hydrogen-assisted decohesion and localized plasticity in dual-phase steel. Acta Mater 2014;70:174–87. https://doi.org/10.1016/j.actamat.2014.01.048.
[38] Svoboda J, Mori G, Prethaler A, Fischer FD. Determination of trapping parameters and the chemical diffusion coefficient from hydrogen permeation experiments. Corrosion Sci 2014;82:93–100. https://doi.org/10.1016/j.corsci.2014.01.002.
[39] Montupet-Leblond F, Corso L, Payet M, Delaporte-Mathurin R, Bernard E, Charles Y, Mougenot J, Vartanian S, Hodille EA, Grisolia C. Permeation and trapping of hydrogen in Eurofer97. Nucl. Mater. Energy. 2021;29:101062. https://doi.org/10.1016/j.nme.2021.101062.
[40] Rhode M, Nietzke J, Mente T, Richter T, Kannengiesser T. Characterization of hydrogen diffusion in offshore steel S420G2+M multi-layer submerged arc welded joint. J Mater Eng Perform 2022. https://doi.org/10.1007/s11665-022-06679-7.
[41] Svoboda J, Fischer FD. Modelling for hydrogen diffusion in metals with traps revisited. Acta Mater 2012;60:1211–20. https://doi.org/10.1016/j.actamat.2011.11.025.
[42] Drexler A, Bergmann C, Manke G, Kokotin V, Mraczek K, Pohl M, Ecker W. On the local evaluation of the hydrogen susceptibility of cold-formed and heat treated advanced high strength steel (AHSS) sheets. Mater Sci Eng 2021;800:140276. https://doi.org/10.1016/j.msea.2020.140276.
[43] Pressouyre GM. A classification of hydrogen traps in steel. Metall Trans A 1979;10:1571–3. https://doi.org/10.1007/BF02812023.
[44] Kholtobina AS, Pippan R, Romaner L, Scheiber D, Ecker W, Razumovskiy VI. Hydrogen trapping in bcc iron. Materials 2020;13:2288. https://doi.org/10.3390/ma13102288.

[45] He S, Popov MN, Ecker W, Pippan R, Razumovskiy VI. A theoretical insight into hydrogen clustering at defects in Ni. Phil Mag Lett 2021;101:68–78. https://doi.org/10.1080/09500839.2020.1851054.
[46] Legrand E, Feaugas X, Bouhattate J. Generalized model of desorption kinetics: characterization of hydrogen trapping in a homogeneous membrane. Int J Hydrogen Energy 2014;39:8374–84. https://doi.org/10.1016/j.ijhydene.2014.03.191.
[47] Rhode M, Mente T, Steppan E, Steger J, Kannengiesser T. Hydrogen trapping in T24 Cr-Mo-V steel weld joints-microstructure effect vs. experimental influence on activation energy for diffusion. Weld World 2018;62:277–87. https://doi.org/10.1007/s40194-017-0546-6.
[48] Raina A, Deshpande VS, Fleck NA. Analysis of thermal desorption of hydrogen in metallic alloys. Acta Mater 2018;144:777–85. https://doi.org/10.1016/j.actamat.2017.11.011.
[49] Raina A, Deshpande VS, Fleck NA. Analysis of electro-permeation of hydrogen in metallic alloys. Philos. Trans. R. Soc. A Math. Phys. Eng. Sci. 2017;375. https://doi.org/10.1098/RSTA.2016.0409.
[50] McNabb A, Foster PK. A new analysis of the diffusion of hydrogen in iron and ferritic steels. Trans. Met. Soc. AIME 1963;227:618–27.
[51] Oriani RA. The diffusion and trapping of hydrogen in steel. Acta Metall 1970;18:147–57. https://doi.org/10.1016/0001-6160(70)90078-7.
[52] Drexler A, Vandewalle L, Depover T, Verbeken K, Domitner J. Critical verification of the Kissinger theory to evaluate thermal desorption spectra. Int J Hydrogen Energy 2021;46:39590–606. https://doi.org/10.1016/j.ijhydene.2021.09.171.
[53] Grabke HJ, Riecke E. Absorption and diffusion of hydrogen in steels. Mater. Tehnol. 2000;34:331–432.
[54] Kiuchi K, McLellan RB. The solubility and diffusivity of hydrogen in well-annealed and deformed iron. Acta Metall 1983;31:961–84. https://doi.org/10.1016/0001-6160(83)90192-X.
[55] Hagi H. Diffusion coefficient of hydrogen in iron without trapping by dislocations and impurities. Mater Trans, JIM 1994;35:112–7. https://doi.org/10.2320/matertrans1989.35.112.
[56] Charles Y, Mougenot J, Gaspérini M. Modeling hydrogen dragging by mobile dislocations in finite element simulations. Int J Hydrogen Energy 2022;47:13746–61. https://doi.org/10.1016/j.ijhydene.2022.02.099.
[57] Sergei S. Atomistic study of hydrogen behavior in Fe in presence of crystal defects. 2021. p. 698.
[58] Svoboda J, Shan YV, Kozeschnik E, Fischer FD. Determination of depths of multiple traps for interstitials and their influence on diffusion kinetics. Model Simulat Mater Sci Eng 2014;22:065015. https://doi.org/10.1088/0965-0393/22/6/065015.
[59] Esteban GA, Perujo A, Sedano LA, Douglas K. Hydrogen isotope di € usive transport parameters in pure polycrystalline tungsten. J Nuclear Mater 2001;295:49–56.
[60] Jebaraj JJM, Morrison DJ, Suni II. Hydrogen diffusion coefficients through Inconel 718 in different metallurgical conditions. Corrosion Sci 2014;80:517–22. https://doi.org/10.1016/j.corsci.2013.11.002.
[61] Barrer R. Diffusion in and through solids. 1st ed. Cambridge, New York: The Universtiy Press, Macmillan; 1941. https://openlibrary.org/books/OL24430943M/Diffusion_in_and_through_solids.
[62] Chen Y-SS, Lu H, Liang J, Rosenthal A, Liu H, Sneddon G, McCarroll I, Zhao Z, Li W, Guo A, Cairney JM. Observation of hydrogen trapping at dislocations, grain boundaries, and precipitates. Science 2020;367:171–5. https://doi.org/10.1126/science.aaz0122.
[63] Gibala R, Counts WA, Wolverton C. The hydrogen cold work peak in BCC iron: revisited, with first principles calculations and implications for hydrogen embrittlement. Mater Res 2018;21:20170868. https://doi.org/10.1590/1980-5373-MR-2017-0868.
[64] McEniry EJ, Hickel T, Neugebauer J. Hydrogen behaviour at twist {110} grain boundaries in α-Fe. Philos. Trans. R. Soc. A Math. Phys. Eng. Sci. 2017;375:20160402. https://doi.org/10.1098/rsta.2016.0402.
[65] Mirzaev DA, Mirzoev AA, Okishev KY, Verkhovykh AV. Ab initio modelling of the interaction of H interstitials with grain boundaries in bcc Fe. Mol Phys 2016;114:1502–12. https://doi.org/10.1080/00268976.2015.1136439.
[66] Asahi H, Hirakami D, Yamasaki S. Hydrogen trapping behavior in vanadium-added steel. ISIJ Int 2003;43:527–33. https://doi.org/10.2355/isijinternational.43.527.
[67] Turk A, San Martín D, Rivera-Díaz-del-Castillo PEJ, Galindo-Nava EI. Correlation between vanadium carbide size and hydrogen trapping in ferritic steel. Scripta Mater 2018;152:112–6. https://doi.org/10.1016/j.scriptamat.2018.04.013.
[68] Schaffner T, Hartmaier A, Kokotin V, Pohl M. Analysis of hydrogen diffusion and trapping in ultra-high strength steel grades. J Alloys Compd 2018;746:557–66. https://doi.org/10.1016/j.jallcom.2018.02.264.
[69] Liu Q, Venezuela J, Zhang M, Zhou Q, Atrens A. Hydrogen trapping in some advanced high strength steels. Corrosion Sci 2016;111:770–85. https://doi.org/10.1016/j.corsci.2016.05.046.
[70] Van den Eeckhout E, De Baere I, Depover T, Verbeken K. The effect of a constant tensile load on the hydrogen diffusivity in dual phase steel by electrochemical permeation experiments. Mater Sci Eng 2020;773:138872. https://doi.org/10.1016/j.msea.2019.138872.
[71] Traxler I, Schimo-Aichhorn G, Muhr A, Commenda C, Jerrar A, Sagl R, Mraczek K, Luckeneder G, Duchaczek H, Stellnberger KH, Rudomilova D, Prošek T, Hassel AW, Hild S. Optimization of metallographic sample preparation for afm/skpfm based phase distinction of complex and dual phase high strength steels. Prakt. Metallogr. Metallogr. 2021;58:308–31. https://doi.org/10.1515/pm-2021-0024.
[72] Du Y, Gao X, Lan L, Qi X, Wu H, Du L, Misra RDK. Hydrogen embrittlement behavior of high strength low carbon medium manganese steel under different heat treatments. Int J Hydrogen Energy 2019;44:32292–306. https://doi.org/10.1016/j.ijhydene.2019.10.103.
[73] Seo HJ, Kim JN, Jo JW, Lee CS. Effect of tempering duration on hydrogen embrittlement of vanadium-added tempered martensitic steel. Int J Hydrogen Energy 2021;46:19670–81. https://doi.org/10.1016/j.ijhydene.2021.03.109.
[74] Díaz A, Zafra A, Martínez-Pañeda E, Alegre JM, Belzunce J, Cuesta II. Simulation of hydrogen permeation through pure iron for trapping and surface phenomena characterisation. Theor Appl Fract Mech 2020;110. https://doi.org/10.1016/j.tafmec.2020.102818.